Stability bounds for the generalized Kadanoff-Baym ansatz in the Holstein dimer

O. Moreno Segura, Y. Pavlyukh, and R. Tuovinen 1

¹Department of Physics, Nanoscience Center, P.O. Box 35, 40014 University of Jyväskylä, Finland ²Institute of Theoretical Physics, Faculty of Fundamental Problems of Technology, Wroclaw University of Science and Technology, 50-370 Wroclaw, Poland

Predicting real-time dynamics in correlated systems is demanding: exact two-time Green's function methods are accurate but often too costly, while the Generalized Kadanoff-Baym Ansatz (GKBA) offers time-linear propagation at the risk of uncontrolled behavior. We examine when and why GKBA fails in a minimal yet informative setting, the Holstein dimer that describes electron-phonon coupling. Using a conserving, fully self-consistent electron-phonon self-energy, we map out parameter regions where GKBA dynamics is stable and where it becomes unstable. We trace the onset of these failures to qualitative changes in the model's ground-state solutions obtained from the full nonequilibrium Green's function theory, thereby providing practical stability bounds for GKBA time evolution. We further show that coupling the dimer to electronic leads can damp and, in part, cure these instabilities. The results supply simple diagnostics and guidelines for reliable GKBA simulations of electron-phonon dynamics.

I. INTRODUCTION

Nonequilibrium dynamics of quantum-correlated many-body systems presents formidable conceptual and computational challenges. A systematic and conserving description is provided by the nonequilibrium Green's function (NEGF) framework based on the Keldysh-Kadanoff-Baym equations (KBE) [1–5]. However, direct two-time solutions of the KBE entail a cubic scaling with the number of time steps, which renders realistic simulations prohibitively expensive for long propagation times or extended parameter scans.

To reduce the computational complexity, the Generalized Kadanoff-Baym Ansatz (GKBA) [6] reconstructs two-time Green's functions from single-time quantities, enabling algorithms with linear scaling in the number of time steps. This favorable scaling has spurred a broad range of developments and applications across closed and open systems [7–12]. At the same time, it has become clear that the GKBA can exhibit uncontrolled behavior in certain regimes: reports include instabilities or unphysical transients in electronic occupations [13, 14], pathologies in electron-boson dynamics [10, 15], and problematic current evolution in open quantum systems [16–19]. These observations motivate a careful assessment of the dynamical stability of GKBA evolutions.

In this work, GKBA stability is analyzed for a paradigmatic electron-phonon setting: the Holstein dimer (see Fig. 1). Focusing on the fully self-consistent and conserving GD approximation for the electron-phonon self-energy [8, 20, 21], the study maps out parameter regions of stable and unstable GKBA dynamics and relates them to known "bifurcations" of the Holstein model's ground-state properties obtained from the full NEGF theory [20]. This correspondence provides practical stability bounds for GKBA time evolution in electron-phonon problems. The analysis is then extended to an open-system setting by coupling the dimer to electronic leads within the wide-band limit approximation (WBLA) [12]. It is found that the tunneling-induced damping can regularize parts of the unstable GKBA regime in the isolated system, in line with the inclusion of quasi-particle effects in related GKBA applications [22–25]. At the same time, caveats associated with energy conservation in open systems apply [26, 27], which provide additional context for the present electron-phonon analysis.

The paper is organized as follows. Section II introduces the Holstein (dimer) model and the governing NEGF+GKBA equations. Section III presents simulations that map stable and unstable regimes across the model's parameter space. Section IV summarizes the main findings and outlines avenues for future work.

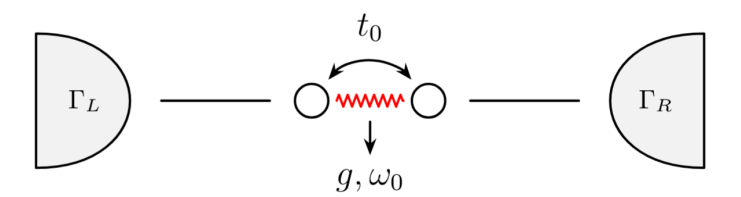


FIG. 1. Schematic of the Holstein dimer coupled to leads. The relative phonon mode—characterized by coupling g and frequency ω_0 —is shown. Γ_{α} ($\alpha = L, R$) denotes the tunneling rate to the leads, and t_0 is the hopping term between sites.

II. THEORY

The Hamiltonian for the model of interacting electrons and phonons (see Fig. 1) studied in this work is the following

$$\hat{H} = -t_0(\hat{d}_1^{\dagger} \hat{d}_2 + \hat{d}_2^{\dagger} \hat{d}_1) + \sum_i \omega_i \hat{a}_i^{\dagger} \hat{a}_i - g \sum_i (\hat{a}_i^{\dagger} + \hat{a}_i) \hat{n}_i, \tag{1}$$

where \hat{d}_i (\hat{a}_i) and \hat{d}_i^{\dagger} (\hat{a}_i^{\dagger}) are the fermionic (bosonic) annihilation and creation operators, respectively. $\hat{n}_i = \hat{d}_i^{\dagger} \hat{d}_i$ is the fermionic number operator. The parameter g denotes the interaction strength between electrons and phonons, t_0 is the characteristic hopping term, and ω_i the phonon frequency. To be consistent with the typical formulation in NEGF [20, 21], we rewrite the phononic and interacting Hamiltonian by introducing the displacement operator $\hat{u}_i \equiv \hat{\phi}_{i,1} = (\hat{a}_i^{\dagger} + \hat{a}_i)/\sqrt{2}$, and momentum operator $\hat{p}_i \equiv \hat{\phi}_{i,2} = i(\hat{a}_i^{\dagger} - \hat{a}_i)/\sqrt{2}$,

$$\hat{H}_{p}(t) = \sum_{\mu\nu} \Omega_{\mu\nu}(t) \hat{\phi}_{\mu} \hat{\phi}_{\nu}, \quad \hat{H}_{e}(t) = \sum_{ij} h_{ij}(t) \hat{d}_{i}^{\dagger} \hat{d}_{j}, \quad \hat{H}_{e-p}(t) = \sum_{\mu,ij} g_{\mu,ij}(t) \hat{d}_{i}^{\dagger} \hat{d}_{j} \hat{\phi}_{\mu}, \tag{2}$$

where we also introduced the one-electron matrix elements h_{ij} . The time dependence of the electron-phonon coupling is due to a switch-on function, which is specified in the next section. The composite index μ combines the phononic mode label i with $\xi = 1, 2$ for displacement and momentum, so that $\mu = (i, \xi)$. The Hamiltonian (1) is recovered by substituting the following relations,

$$h = -t_0 \begin{pmatrix} 0 & 1 \\ 1 & 0 \end{pmatrix}, \quad \Omega_{\mu\nu} \equiv \frac{\omega_i}{2} (\delta_{ij} \delta_{\xi\xi'} + \alpha_{i\xi,j\xi'}), \quad g_{\mu,jk} \equiv -\sqrt{2}g \delta_{\xi,1} \delta_{ij} \delta_{jk}, \tag{3}$$

where the matrix α comes from the commutation relations for the $\hat{\phi}$ fields,

$$[\hat{\phi}_{\mu}, \hat{\phi}_{\nu}] = \alpha_{\mu\nu}, \quad \alpha_{\mu\nu} = \delta_{ij} \begin{pmatrix} 0 & i \\ -i & 0 \end{pmatrix}_{\varepsilon\varepsilon'}.$$
 (4)

The effect of electronic leads is modeled by

$$\hat{H}_{\text{lead}} = \sum_{k\alpha} \epsilon_{k\alpha} \hat{d}_{k\alpha}^{\dagger} \hat{d}_{k\alpha}, \tag{5}$$

$$\hat{H}_{\text{tunneling}}(t) = \sum_{ik\alpha} \left[T_{k\alpha,i}(t) \hat{d}_{k\alpha}^{\dagger} \hat{d}_{i} + \text{H.c.} \right], \tag{6}$$

where $\epsilon_{k\alpha}$ is the energy dispersion relation for the k-th state in the α -th lead, and $T_{k\alpha,i}$ is the tunneling matrix element between the lead and dimer states. The latter object is time-dependent, similar to g, with a switch-on function specified below.

In the context of NEGF, we are interested in the one-particle Green's functions (GFs), and as we work here under the fully self-consistent Born approximation, i.e., the so-called GD approximation [8, 9], we take into account the electronic and phononic GFs, with lesser and greater components

$$G_{ij}^{<}(t,t')=i\langle\hat{d}_{j}^{\dagger}(t')\hat{d}_{i}(t)\rangle,\quad G_{ij}^{>}(t,t')=-i\langle\hat{d}_{i}(t)\hat{d}_{j}^{\dagger}(t')\rangle,\quad D_{\mu\nu}^{<}(t,t')=D_{\nu\mu}^{>}(t',t)=-i\langle\Delta\hat{\phi}_{\nu}(t')\Delta\hat{\phi}_{\mu}(t)\rangle, \tag{7}$$

where $\Delta \hat{\phi}_{\nu}(t) \equiv \hat{\phi}_{\nu}(t) - \langle \hat{\phi}_{\nu}(t) \rangle$ is the fluctuation operator and $\langle \hat{\phi}_{\nu}(t) \rangle = \phi_{\nu}(t)$ is the expectation value of the phononic field. These two correlators satisfy their corresponding Kadanoff-Baym equations in matrix representation [8]:

$$[i\partial_t - h^{\mathrm{e}}(t)]G^{\lessgtr}(t, t') = [\Sigma^{\lessgtr} \cdot G^A + \Sigma^R \cdot G^{\lessgtr}](t, t'), \tag{8}$$

$$[i\partial_t - h^{\mathrm{p}}(t)]D^{\lessgtr}(t, t') = \alpha \left[\Pi^{\lessgtr} \cdot D^A + \Pi^R \cdot D^{\lessgtr}\right](t, t'), \tag{9}$$

where superscripts A and R stand for the advanced and retarded components, respectively, and $[a \cdot b](t,t') \equiv \int d\bar{t} \ a(t,\bar{t})b(\bar{t},t')$ denotes a real-time convolution. The electronic self-energy $\Sigma = \Sigma_c + \Sigma_{\rm em}$ consists of the correlation Σ_c and embedding $\Sigma_{\rm em}$ parts. The former accounts for the electron-phonon interaction, while the latter for the system-leads coupling. The electronic Hamiltonian $h^e(t)$ includes the time-local mean-field contribution, so it is the one-body Hamiltonian and the phononic potential, $h^e_{ij}(t) = h_{ij}(t) + \sum_{\mu} g_{\mu,ij}(t)\phi_{\mu}(t)$. The term Π is the phononic self-energy, and $h^p \equiv \alpha(\Omega + \Omega^T)$ the effective phononic Hamiltonian.

The equation of motion (EOM) for the electronic density matrix $\rho_{\rm e}(t) = -iG^{<}(t,t)$ and the phononic density matrix $\rho_{\rm p}(t) = iD^{<}(t,t)$ can be obtained from Eqs. (8), (9) and their adjoints, and taking the limit t = t',

$$i\frac{d}{dt}\rho_{\rm e}(t) = [h^{\rm e}(t)\rho_{\rm e}(t) - iI_{\rm c}(t) - iI_{\rm em}(t)] - \text{H.c.},$$
 (10a)

$$i\frac{d}{dt}\rho_{\rm p}(t) = [h^{\rm p}(t)\rho_{\rm p}(t) + iI_{\rm p}(t)] - \text{H.c.},$$
 (10b)

where I_c , I_{em} , and I_p are the collision integrals, which come from the convolution of the corresponding self-energies and the GFs. To make the collision integrals functionals of the density matrices $\rho_e(t)$ and $\rho_p(t)$ we employed the GKBA [8]

$$G^{\lessgtr}(t,t') = \mp \left[G^R(t,t')\rho_{\rm e}^{\lessgtr}(t') - \rho_{\rm e}^{\lessgtr}(t)G^A(t,t') \right],\tag{11}$$

$$D^{\lessgtr}(t,t') = D^R(t,t')\alpha \rho_{\mathsf{D}}^{\lessgtr}(t') - \rho_{\mathsf{D}}^{\lessgtr}(t)\alpha D^A(t,t'),\tag{12}$$

and we approximate the retarded and advanced GFs at the mean-field level

$$G^{R}(t,t') = -i\theta(t-t')\mathcal{T}\left[\exp\left(-i\int_{t'}^{t} d\bar{t}[h^{e}(\bar{t}) - \frac{i}{2}\Gamma(\bar{t})]\right)\right],\tag{13}$$

$$D^{R}(t,t') = -i\alpha\theta(t-t')\mathcal{T}\left[\exp\left(-i\int_{t'}^{t} d\bar{t} \ h^{p}(\bar{t})\right)\right],\tag{14}$$

with $\Gamma(t) \equiv \sum_{\alpha} s_{\alpha}^{2}(t) \Gamma_{\alpha}$, where $s_{\alpha}(t)$ is the switch-on function for the coupling between the lead α and the system, and Γ_{α} is the line-width matrix of lead α at the WBLA level [12]:

$$\Gamma_{\alpha,ij} = 2\pi \sum_{k} T_{i,k\alpha} \delta(\mu - \epsilon_{k\alpha}) T_{k\alpha,j}, \tag{15}$$

where μ is the chemical potential. For $\Gamma = 0$, G^R is reduced to the propagator for closed systems, which is used when the leads are disconnected ($\Sigma_{\rm em} = 0$).

The time-linear method is constructed by first rewriting the collision integrals I_c and I_p in terms of a higher-order correlator \mathcal{G}^{e-p} (approximated here at the GD level), and then deriving its EOM as introduced in Refs. 8, 9. A similar procedure is applied to I_{em} by defining an embedding correlator \mathcal{G}^{em} under the wide-band limit approximation and finding its EOM, as developed in Ref. 12. Based on these considerations, we rewrite Eq. (10a) for $\rho_e(t)$ as

$$i\frac{d}{dt}\rho_{e,ij}(t) = \left(\left[h_{\text{eff}}^{e}(t)\rho_{e}(t) \right]_{ij} + \frac{i}{4}\Gamma_{ij}(t) + \sum_{l\alpha} s_{\alpha}(t) \frac{\eta_{l}}{\beta} \Gamma_{\alpha,ij} \mathcal{G}_{l\alpha}^{em}(t) + \sum_{\mu,k} g_{\mu,ik}(t) \mathcal{G}_{\mu,kj}^{e-p}(t) \right) - \text{H.c.},$$
(16)

where $h_{\text{eff}}^{\text{e}}(t) \equiv h^{\text{e}}(t) - i \Gamma(t)/2$ is the effective Hamiltonian, η_l arise from the pole expansion of the Fermi function [28], and β denotes the inverse temperature. Similarly, Eq. (10b) for $\rho_{\text{p}}(t)$ can be rewritten as

$$i\frac{d}{dt}\rho_{p,\mu\nu}(t) = \left([h^{p}(t)\rho_{p}(t)]_{\mu\nu} + \sum_{ij} \bar{g}_{\mu,ij}(t)\mathcal{G}_{\nu,ji}^{e-p}(t) \right) - \text{H.c.},$$
(17)

where $\bar{g}_{\mu,ij} = \sum_{\nu} \alpha_{\mu\nu} g_{\nu,ij}$. Equations (16) and (17) must be coupled to the EOM for the higher-order electron-phonon correlator

$$i\frac{d}{dt}\mathcal{G}_{\mu,ij}^{\text{e-p}}(t) = -\Psi_{\mu,ij}(t) + \sum_{\sigma} h_{\mu\sigma}^{\text{p}}(t)\mathcal{G}_{\sigma,ij}^{\text{e-p}}(t) + \sum_{k} [h_{ik}^{\text{e}}(t)\mathcal{G}_{\mu,kj}^{\text{e-p}}(t) - \mathcal{G}_{\mu,ik}^{\text{e-p}}(t)h_{kj}^{\text{e}}(t)],$$
(18)

where $\Psi_{\mu,ij}(t) = \Psi_{\mu,ij}^{>}(t) - \Psi_{\mu,ij}^{<}(t)$ with $\Psi_{\mu,ij}^{\lessgtr}(t) = \sum_{\nu,sq} \rho_{\mathrm{p},\mu\nu}^{\lessgtr}(t) \rho_{\mathrm{e},is}^{\lessgtr}(t) g_{\nu,sq}(t) \rho_{\mathrm{e},qj}^{\gtrless}(t)$. Equation (16) is also coupled to the EOM of the embedding correlator

$$i\frac{d}{dt}\mathcal{G}_{l\alpha}^{\text{em}}(t) = -s_{\alpha}(t) - \mathcal{G}_{l\alpha}^{\text{em}}(t) \left(h_{\text{eff}}^{\text{eff}}(t) - V_{\alpha}(t) - \mu + i\frac{\zeta_{l}}{\beta} \right), \tag{19}$$

where $V_{\alpha}(t)$ is the bias-voltage profile and ζ_l result from the pole expansion of the Fermi function [28]. Additionally, the evolution of the expectation values ϕ_{μ} , which enter $h^{\rm e}$, must be taken into account

$$i\frac{d}{dt}\phi_{\mu}(t) = \sum_{\nu} h_{\mu\nu}^{\mathrm{p}}(t)\phi_{\nu}(t) + \sum_{ij,\sigma} \alpha_{\mu\sigma}g_{\sigma,ij}(t)\rho_{\mathrm{e},ji}(t). \tag{20}$$

This set of coupled ordinary differential equations, (16), (17), (18), (19), and (20), defines the framework used to describe the system. Within this formalism, we evaluate observables such as the electronic natural occupation (i.e., the eigenvalues of ρ_e), the phonon number, and the interaction energies. The phonon number is given by

$$n_{p,i}(t) = \frac{1}{2} \left(\sum_{\xi} \left(\rho_{p,i\xi,i\xi}(t) + \left[\phi_{i\xi}(t) \right]^2 \right) - 1 \right).$$
 (21)

The total energy is computed from the mean-field contributions of the electronic, phononic, and electron-phonon terms, together with the correlation energies, as follows

$$E = E_{e}(t) + E_{p}(t) + E_{e-p}(t) + E_{e,c}(t) + E_{p,c}(t),$$
(22)

where each term is calculated according to

$$E_{e}(t) = \text{Tr}\left[h(t)\rho_{e}(t)\right] \tag{23}$$

$$E_{\mathbf{p}}(t) = \text{Tr}\left[\Omega(t)\Lambda(t)\right],\tag{24}$$

$$E_{e-p}(t) = \text{Tr}\left[h_{e-p}(t)\rho_{e}(t)\right], \tag{25}$$

$$E_{\rm e,c}(t) = -\frac{i}{4} \text{Tr} \left[I_{\rm c}(t) - I_{\rm c}^{\dagger}(t) \right], \tag{26}$$

$$E_{p,c}(t) = \frac{i}{4} \text{Tr} \left[\alpha I_p(t) + (\alpha I_p(t))^T \right], \tag{27}$$

where $h_{e-p,ij}(t) = \sum_{\mu} g_{\mu,ij}(t)\phi_{\mu}(t)$ and $\Lambda_{\mu\nu} = \rho_{p,\mu\nu}(t) + \phi_{\mu}(t)\phi_{\nu}(t)$. The correlation energies are expressed in terms of the collision integrals for readability; however, they are evaluated using the correlators \mathcal{G}^{em} and \mathcal{G}^{e-p} , approximated as described above. All our calculations following this scheme are performed with the CHEERS code [29].

III. RESULTS

The system defined in Eq. (1) is characterized by two dimensionless parameters, the adiabatic ratio γ and the effective interaction λ , given by

$$\gamma \equiv \frac{\omega_0}{t_0}, \quad \lambda \equiv \frac{g^2}{\omega_0 t_0}.$$
 (28)

In the following, the hopping term is set as the energy unit $(t_0 = 1)$; hence γ is determined solely by the phonon frequency ω_0 . Times are thus expressed in units of inverse hoppings. In addition, the electronic particle number is fixed to one.

To start our analysis, we calculate the total energy of the isolated system ($\Sigma_{\rm em}=0$) as a function of the effective interaction for several values of the adiabatic ratio. An important feature we control in our simulations is the time-dependent coupling, where starting from the uncoupled electron–phonon system, it follows the switching protocol $g(t)=g\cos^2\left(\frac{\pi t}{2t_i}\right)$ for t<0. For $t\geq 0$, g(t)=g. Therefore, we present different cases by varying the initial time t_i of the simulation, and all cases are propagated until $t_f=50$. Figure 2 shows two representative cases that illustrate the regimes $\gamma<0.9$ and $\gamma>0.9$, where the total energy is taken to be its value at t_f . An example of a time-dependent calculation is shown in Fig. 4, discussed in detail below.

The case $\gamma = 0.5$ (Fig. 2a) is completely stable, and the energy behavior is in agreement with the results presented in Ref. 20; the two distinct lines arise because $t_i = -20$ is insufficient to reach a steady state at large λ , the other cases converge to the same value and therefore overlap. By contrast, $\gamma = 1.1$ (Fig. 2b) corresponds to a typical unstable case, where the lower critical value of the effective interaction is found around $\lambda \approx 0.75$. The extent of the unstable range depends on the initial time, being the most unstable case $t_i = -200$, which can be related to the longer

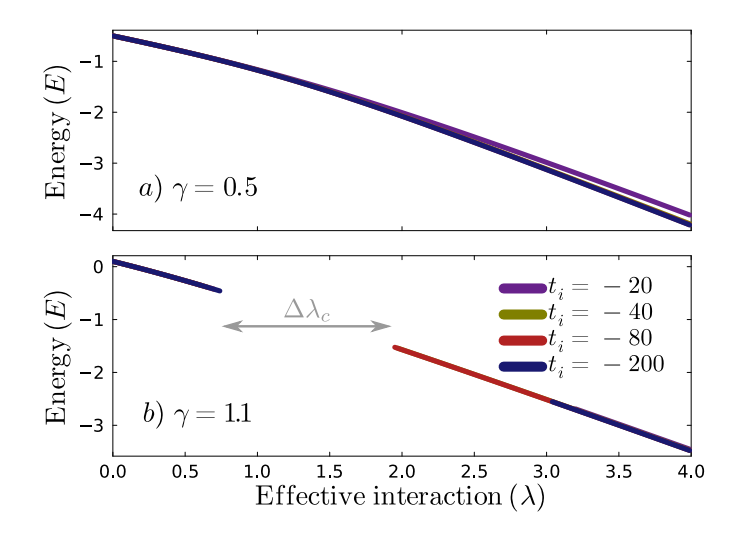


FIG. 2. Total energy as a function of the effective interaction for different switching times. The region in panel (b) where the curves show discontinuities—blank gaps—corresponds to instabilities. The difference between the upper and lower critical values is indicated by $\Delta \lambda_c$ for the case $t_i = -80$.

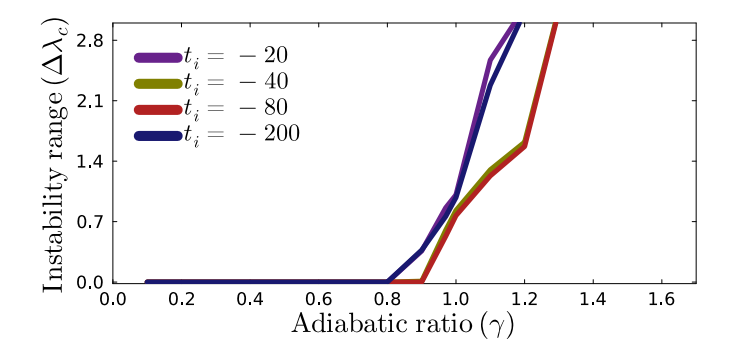


FIG. 3. Unstable range of the effective interaction as a function of the adiabatic ratio for several switching times. Instability is signaled by the curves deviating from zero.

propagation window. The situations for $t_i = -40$ and $t_i = -80$ are approximately similar (the two curves almost overlap throughout), with the latter resulting in the most stable case.

In Fig. 3, we show the instability range $\Delta \lambda_c$ of the effective interaction—defined as the difference between the lower and upper critical values of λ (cf. Fig. 2b)—as a function of the adiabatic ratio, thereby characterizing the emergent instabilities in the parameter space (λ, γ) . For all $\gamma \leq 0.8$, the four cases are stable within the explored range $0 \leq \lambda \leq 4$. Conversely, once the adiabatic ratio is larger than 0.9, all the cases start to exhibit instabilities, which grow exponentially fast. It is worth emphasizing that when the effective interaction is smaller than approximately 0.75, the simulations are stable for all values of the adiabatic ratio studied here $(\gamma \leq 4)$.

Our results for the unstable range of the effective interaction resemble the behavior of the critical values in λ associated with the emergence of an asymmetric solution reported in Ref. 20, based on the full KBE theory. As shown by Säkkinen *et al.* [20], at the mean-field level, this solution appears as a bifurcation produced by symmetry breaking, independent of the adiabatic ratio, whereas for the fully self-consistent GD approximation, the asymmetric solution emerges discontinuously and has a strong dependence on the adiabatic ratio. In our case, although we employ the GD approach, we close the GKBA with mean-field propagators, Eqs. (13) and (14), which leads to an interplay of both scenarios. First, we find that the lower unstable value of λ is approximately constant (≈ 0.75); and second, the upper unstable value of λ is strongly dependent on γ . Therefore, this is an evident connection between the existence of an asymmetric solution to the instabilities in the GKBA for this model.

We continue by studying the dynamics in the system through the electronic natural occupation and the phononic occupation number. To this end, we present a representative case that can be either stable or unstable depending on the initial time t_i . These cases are informative because they capture the typical behavior of both regimes. Figure 4 shows the population dynamics for $\lambda = 2$ and $\gamma = 1.1$, which correspond to the partially stable/unstable regime identified

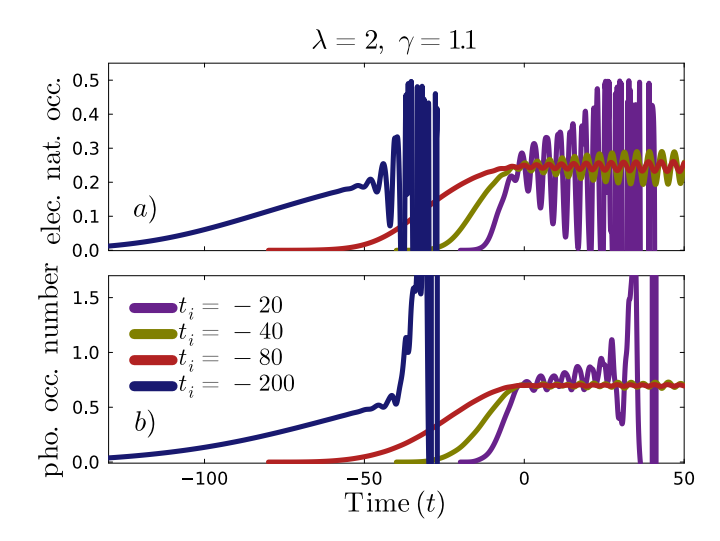


FIG. 4. Electronic natural occupation number and phononic occupation number as a function of time for different switching times. These temporal evolutions correspond to those of higher adiabatic ratios γ in Fig. 2b.

in Fig. 2b. For the identified stable cases in our time window $(t_f = 50)$, $t_i = -40$ and $t_i = -80$, the occupations approach a finite value at t = 0 and subsequently exhibit small oscillations around it. For the unstable situations, two different scenarios occur, but both are clearly related to the divergence in the phononic occupation number. For $t_i = -20$, the dynamics break down at positive times after a period of strong oscillations in the electronic natural occupation. In contrast, for $t_i = -200$ the simulation breaks down already at negative times (during the switching stage), where a shorter period of oscillations in the natural occupation is followed by a sudden increase in the phononic occupation that triggers the numerical failure.

Previous work [30] has shown that adding a velocity damping term stabilizes correlated electron dynamics in a Hubbard dimer. Here, we investigate whether coupling the Holstein dimer system to electronic leads, described within the WBLA, can achieve a similar stabilization of the electron-phonon dynamics. Therefore, in this part we open the system ($\Sigma_{\rm em} \neq 0$), and the embedding correlator in Eq. (19) becomes nonzero. This is done by connecting one lead labeled $\alpha = L$ to the site on the left and the other labeled $\alpha = R$ to the site on the right (see Fig. 1). The chemical potential is fixed at the middle of the energy gap of the uncontacted system. The inverse temperature parameter is fixed to $\beta = 10$. As shown in Fig. 5, applying the embedding scheme to the case discussed above effectively removes the instabilities. The case presented here is for zero voltage bias [$V_{\alpha} = 0$ in Eq. (19)] and a line-width matrix with norm $\Gamma = 0.1$.

The effective suppression of spurious oscillations—and the resulting divergences—is evident from the explicit form of the electronic propagator $G^R(t,t')$ in Eq. (13), and the role of Γ , which produces an exponential decay. In this sense, it is intuitive to follow the system's dependence on Γ as a control parameter. It is found that for more complicated cases (stronger instabilities), such as $\gamma > 1.4$, the Γ required to stabilize the simulation must be larger. The simulations for these open systems were propagated up to $t_f = 8000$ and remained stable. However, although this provides an alternative to control the instabilities, we identify an unphysical increase in the phonon number: unlike the electronic natural occupation, which reaches a steady finite value, the phononic occupation continues to grow slowly. We have tested (not shown) that the slope of the phonon occupation number increases with Γ . This could be related to the larger broadening of the electronic levels (reducing Pauli blocking) increasing the energy accumulation in the phonon modes. In our model, the phonon sector lacks its own dissipation channel, but we will defer more thorough investigations of this effect to future work. We also caution that once Γ becomes comparable to the intrinsic energy scales (t_0, ω_0, g) of the dimer, the open and isolated problems are no longer directly comparable: increasing Γ does not merely regularize the dynamics but opens a lead-mediated scattering channel and enables net energy exchange with the leads, thus modifying the physical evolution.

IV. CONCLUSION

This work has examined the dynamical stability of the GKBA for a minimal yet physically meaningful electronphonon problem, the Holstein dimer. Owing to its simplicity and analytical transparency, the dimer enables a controlled study of GKBA evolutions. Within the conserving GD approximation, regions of stable and unstable

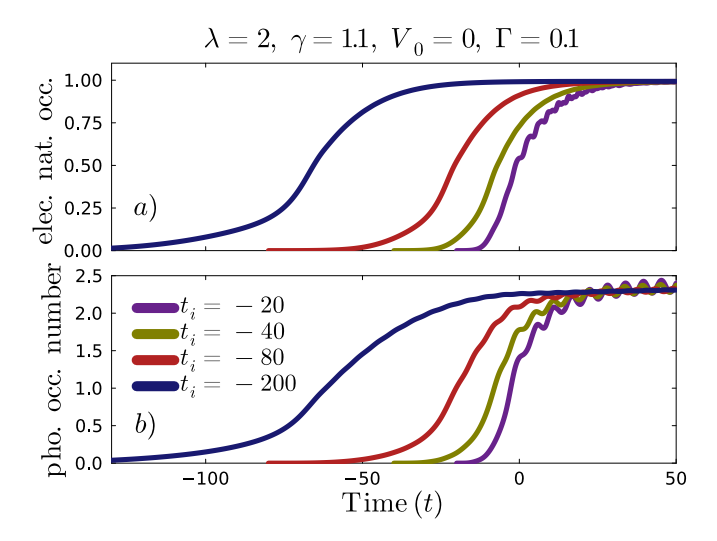


FIG. 5. Electronic natural occupation number and phononic occupation number as a function of time for the system connected to leads. Results are shown for several switching times.

GKBA dynamics were identified. The onset of instability in time evolution coincides with ground-state "bifurcations", which were previously characterized using the full NEGF theory for the same model, as qualitative changes in the stationary solutions [20]. This correspondence yields practical bounds for reliable GKBA simulations of electron-phonon dynamics.

Coupling the dimer to WBLA leads was shown to mitigate parts of the unstable regime through dissipative damping, echoing quasi-particle effects noted in GKBA transport applications [31, 32]. While such open-system regularization can be beneficial, it necessarily introduces energy exchange with the environment and must be assessed with the conserving properties of the chosen propagators in mind [12, 22, 26]. Altogether, the results map stability domains for GKBA in a canonical electron-phonon setting and suggest concrete diagnostics for anticipating instabilities. Future studies can extend these ideas to larger lattices and nonequilibrium transport setups with structured, non-wide band reservoirs [18, 19], thereby testing the generality of the identified stability bounds and refining GKBA formulations for robust electron-boson dynamics.

ACKNOWLEDGMENTS

O.M.S. and R.T. acknowledge the financial support of the Jane and Aatos Erkko Foundation (Project EffQSim). R.T. further acknowledges the Research Council of Finland through the Finnish Quantum Flagship (Project No. 359240).

^[1] L. V. Keldysh, Diagram Technique for Nonequilibrium Processes, Sov. Phys. JETP 20, 1018 (1965).

^[2] L. P. Kadanoff and G. Baym, Quantum Statistical Mechanics (W. A. Benjamin, New York, 1962).

^[3] P. Danielewicz, Quantum theory of nonequilibrium processes, i, Ann. Phys. (N. Y.) 152, 239 (1984).

^[4] G. Stefanucci and R. van Leeuwen, *Nonequilibrium Many-Body Theory of Quantum Systems: A Modern Introduction*, 2nd ed. (Cambridge University Press, 2025).

^[5] K. Balzer and M. Bonitz, Nonequilibrium Green's Functions Approach to Inhomogeneous Systems (Springer Berlin Heidelberg, 2013).

 ^[6] P. Lipavský, V. Špička, and B. Velický, Generalized kadanoff-baym ansatz for deriving quantum transport equations, Phys. Rev. B 34, 6933 (1986).

^[7] N. Schlünzen, J.-P. Joost, and M. Bonitz, Achieving the scaling limit for nonequilibrium green functions simulations, Phys. Rev. Lett. 124, 076601 (2020).

^[8] D. Karlsson, R. van Leeuwen, Y. Pavlyukh, E. Perfetto, and G. Stefanucci, Fast green's function method for ultrafast electron-boson dynamics, Phys. Rev. Lett. 127, 036402 (2021).

- [9] Y. Pavlyukh, E. Perfetto, D. Karlsson, R. van Leeuwen, and G. Stefanucci, Time-linear scaling nonequilibrium green's function methods for real-time simulations of interacting electrons and bosons. i. formalism, Phys. Rev. B 105, 125134 (2022).
- [10] Y. Pavlyukh, E. Perfetto, D. Karlsson, R. van Leeuwen, and G. Stefanucci, Time-linear scaling nonequilibrium green's function method for real-time simulations of interacting electrons and bosons. ii. dynamics of polarons and doublons, Phys. Rev. B 105, 125135 (2022).
- [11] K. Balzer, N. Schlünzen, H. Ohldag, J.-P. Joost, and M. Bonitz, Accelerating nonequilibrium green function simulations with embedding self-energies, Phys. Rev. B 107, 155141 (2023).
- [12] R. Tuovinen, Y. Pavlyukh, E. Perfetto, and G. Stefanucci, Time-linear quantum transport simulations with correlated nonequilibrium green's functions, Phys. Rev. Lett. 130, 246301 (2023).
- [13] S. Hermanns, N. Schlünzen, and M. Bonitz, Hubbard nanoclusters far from equilibrium, Phys. Rev. B 90, 125111 (2014).
- [14] J.-P. Joost, N. Schlünzen, H. Ohldag, M. Bonitz, F. Lackner, and I. Březinová, Dynamically screened ladder approximation: Simultaneous treatment of strong electronic correlations and dynamical screening out of equilibrium, Phys. Rev. B 105, 165155 (2022).
- [15] G. Stefanucci and E. Perfetto, Semiconductor electron-phonon equations: A rung above Boltzmann in the many-body ladder, SciPost Phys. 16, 073 (2024).
- [16] A. Kalvová, B. Velický, and V. Špička, Beyond the generalized kadanoff-baym ansatz, Phys. Status Solidi B 256, 1800594 (2019).
- [17] A. Kalvová, V. Špička, B. Velický, and P. Lipavský, Dynamical vertex correction to the generalized kadanoff-baym ansatz, Europhys. Lett. 141, 16002 (2023).
- [18] Y. Pavlyukh and R. Tuovinen, Open system dynamics in linear time beyond the wide-band limit, Phys. Rev. B 111, L241101 (2025).
- [19] R. Tuovinen and Y. Pavlyukh, Thermoelectric energy conversion in molecular junctions out of equilibrium, PRX Energy 4, 043003 (2025).
- [20] N. Säkkinen, Y. Peng, H. Appel, and R. van Leeuwen, Many-body green's function theory for electron-phonon interactions: Ground state properties of the holstein dimer, J. Chem. Phys. 143, 234101 (2015).
- [21] N. Säkkinen, Y. Peng, H. Appel, and R. van Leeuwen, Many-body green's function theory for electron-phonon interactions: The kadanoff-baym approach to spectral properties of the holstein dimer, J. Chem. Phys. 143, 234102 (2015).
- [22] M. Bonitz, D. Kremp, D. C. Scott, R. Binder, W. D. Kraeft, and H. S. Köhler, Numerical analysis of non-markovian effects in charge-carrier scattering: one-time versus two-time kinetic equations, J. Phys. Condens. Matter 8, 6057 (1996).
- [23] F. Jahnke, M. Kira, and S. W. Koch, Linear and nonlinear optical properties of excitons in semiconductor quantum wells and microcavities, Z. Phys. B **104**, 559 (1997).
- [24] G. Pal, Y. Pavlyukh, H. C. Schneider, and W. Hübner, Conserving quasiparticle calculations for small metal clusters, Eur. Phys. J. B 70, 483 (2009).
- [25] C. Makait, F. B. Fajardo, and M. Bonitz, Time-dependent charged particle stopping in quantum plasmas: testing the g1–g2 scheme for quasi-one-dimensional systems, Contrib. Plasma Phys. 63, e202300008 (2023).
- [26] S. Latini, E. Perfetto, A.-M. Uimonen, R. van Leeuwen, and G. Stefanucci, Charge dynamics in molecular junctions: Nonequilibrium green's function approach made fast, Phys. Rev. B 89, 075306 (2014).
- [27] M. Bonitz, K. Balzer, N. Schlünzen, M. R. Rasmussen, and J.-P. Joost, Ion impact induced ultrafast electron dynamics in finite graphene-type hubbard clusters, Phys. Status Solidi B **256**, 1800490 (2019).
- [28] J. Hu, R.-X. Xu, and Y. Yan, Communication: Padé spectrum decomposition of fermi function and bose function, J. Chem. Phys. 133, 101106 (2010).
- [29] Y. Pavlyukh, R. Tuovinen, E. Perfetto, and G. Stefanucci, Cheers: A linear-scaling kbe+gkba code, Phys. Status Solidi B **261**, 2300504 (2024).
- [30] Y. Pavlyukh, Nonequilibrium dynamics of the hubbard dimer, Phys. Status Solidi B 261, 2300510 (2024).
- [31] R. Tuovinen, D. Golež, M. Eckstein, and M. A. Sentef, Comparing the generalized kadanoff-baym ansatz with the full kadanoff-baym equations for an excitonic insulator out of equilibrium, Phys. Rev. B 102, 115157 (2020).
- [32] R. Tuovinen, R. van Leeuwen, E. Perfetto, and G. Stefanucci, Electronic transport in molecular junctions: The generalized kadanoff-baym ansatz with initial contact and correlations, J. Chem. Phys. 154, 094104 (2021).